Available online at www.sciencedirect.com
ScienceDirect
Journal of Power Sources 162 (2006) 1122–1129
JOURNAL OF POWER SOURCES
www.elsevier.com/locate/jpowsour

Evaluating the enhanced performance of a novel wave-like form gas flow channel in the PEMFC using the field synergy principle

Jenn-Kun Kuo, Cha'o-Kuang Chen *

Department of Mechanical Engineering, National Cheng Kung University, No. 1 Ta-Hsueh Road, Tainan 70101, Taiwan

Received 28 June 2006; received in revised form 22 July 2006; accepted 24 July 2006
Available online 1 September 2006

Abstract

This study performs numerical simulations to evaluate the convective heat transfer performance and velocity flow characteristics of a novel gas flow channel with a wave-like form designed to enhance the performance of Proton Exchange Membrane Fuel Cells (PEMFCs). To restrict the current simulations to two-dimensional incompressible flows, the flow regime is assumed to be laminar with a low Reynolds number of approximately 200. The numerical results show that compared to a conventional straight gas flow channel, the wave-like geometry of the proposed gas flow channel increases the mean Nusselt number by a factor of approximately two. Furthermore, the periodic wave-like structure increases the gas flow velocity in the channel and hence improves the catalysis reaction performance in the catalyst layer. Finally, the results show that the wave-like geometry of the gas flow channel reduces the included angle between the velocity vector and the temperature gradient. Hence, the present numerical results are consistent with the field synergy principle, which states that the convective heat transfer is enhanced when the velocity vector and temperature gradient are closely aligned with one another.

Keywords: Field synergy principle; PEMFC; Gas flow channel; Heat transfer; Bipolar plates

1. Introduction

Proton exchange membrane fuel cells (PEMFCs) represent a viable alternative power source for various applications. However, to satisfy the requirements for compactness, low cost, and high power density, performance and stability, respectively, various aspects of the PEMFC must be optimized. Many researchers [1–9] have used mathematical models to examine the relationship between the cell voltage of the PEMFC and the current density under various operating conditions. However, the impact on the PEMFC performance of the complex interactions between the electrochemical reactions, hydrodynamic effects, and multicomponent transport mechanisms in the gas flow channels of the fuel cell have thus far received comparatively little attention.

Drawing an analogy between heat convection and heat conduction, Guo et al. [10,11] studied the mechanisms of convective heat transfer and proposed a novel approach for enhancing convective heat transfer under a parabolic fluid flow structure. Guo proposed that under such a flow structure, the convection term can be transformed into a dot product of the velocity vector and the temperature gradient. The convective heat transfer can then be enhanced by raising the value of the integral of the convective term over the thermal boundary layer. The aim of this novel approach is to improve the uniformity of the velocity and temperature profiles and to reduce the included angle between them. Guo et al. [10] referred to this approach as the field synergy (coordination) principle. In a later series of studies, Tao et al. [12,13] extended this concept from parabolic to elliptic fluid flows and to other transport phenomena.

Wang and Chen [14] performed a numerical investigation into the forced convection of flows through a periodic array of a wave-like channel. The results revealed that the flow was characterized by a highly complex flow-pattern, comprising a strong forward flow and oppositely directed re-circulating flows. The gas flow channels in conventional PEMFCs have a straight geometry. However, in an attempt to improve the performance of these fuel cells, this study presents a novel gas flow channel with a periodic wave-like geometry. This unique geometry is designed to increase the gas flow within the channel in order to improve the catalysis reaction performance in the gas diffusion layer.

* Corresponding author. Tel.: +886 6 2757575x62140; fax: +886 6 2342081.
E-mail address: ckchen@mail.ncku.edu.tw (C.-K. Chen).

0378-7753/$ – see front matter © 2006 Elsevier B.V. All rights reserved.
doi:10.1016/j.jpowsour.2006.07.053

Nomenclature

A	convection heat transfer area
c_p	specific heat capacity
D_h	hydraulic diameter
f	frictional factor
h	convection heat transfer coefficient
$\dot{m}$	mass flow rate
Nu	Nusselt number
Q	heat transfer rate
p	pressure
Pr	Prandtl number
Δp	pressure drop
Re	Reynolds number
T	temperature
∇T	temperature gradient
ΔT	temperature difference
u	velocity in axial direction
v	velocity in vertical direction
U	maximum velocity in inlet
$\|U\|$	average velocity
x, y	coordinate system

Greek symbols

ε	porosity
k	thermal conductivity
θ	intersection angle between velocity and temperature gradient
ρ	density

Subscripts

in	inlet, initial
m	mean
max	maximum
min	minimum
out	outlet, outer
w	wall

Furthermore, the wave-like geometry significantly improves the heat transfer performance of the bipolar plate in dissipating the heat generated during the catalysis reaction. The enhanced flow velocity and heat transfer characteristics of the proposed gas flow channel are demonstrated in a series of numerical simulations. Finally, the improved heat transfer performance of the novel gas flow channel is investigated from the perspective of the field synergy principle.

2. Overview of field synergy principle

Fig. 1 presents schematic illustrations of the cross-section and side view of the current bipolar plate comprising gas flow channels with a novel wave-like form. In this configuration the cross-section and hydraulic diameter (0.015 m) of the gas flow channels are identical. The gas diffusion layer has a porosity of $\varepsilon = 0.5$ and a thickness of 300 μm. The gas flow channel has a length of 0.1 m and the bipolar plate side of the channel has a wave-like form with a period of 0.01 m. The flow of the hydrogen gas in the channel is assumed to be laminar with a low Reynolds number of 200, which is typical of that specified in fuel cells designed for aeronautical and automotive applications.

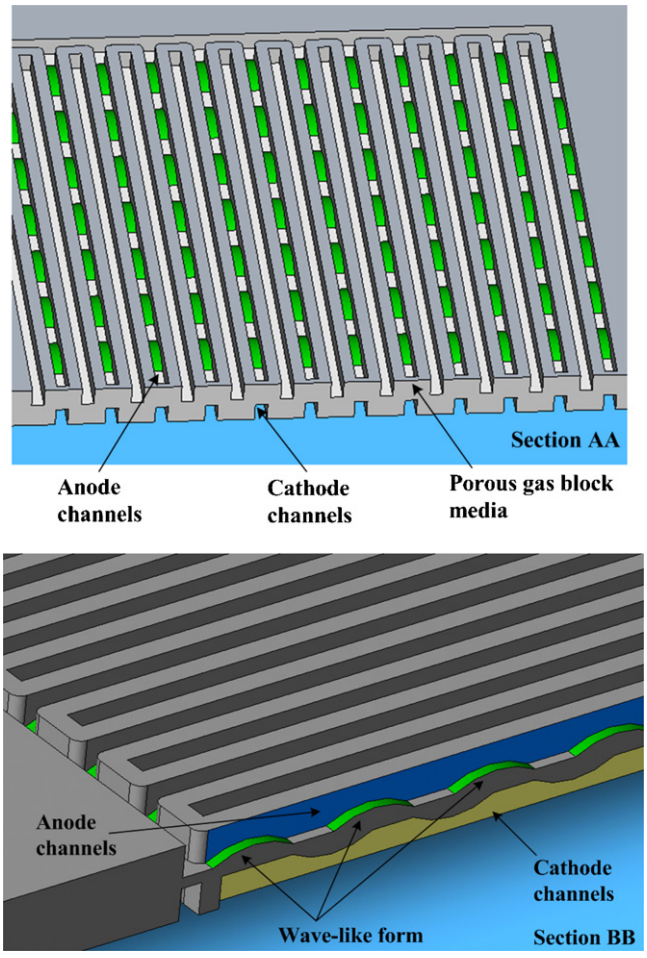

Fig. 1. Cross-section and side view of gas flow channel with periodic wave-like geometry in bipolar plate of a PEMFC.

Fig. 2 presents a cross-section of the current 2-D computational domain. For simplicity, and with no loss of generality, the dimension normal to the cross-section is assumed to be unity. For the case of a steady state elliptic flow of a fluid with constant properties, the energy governing equation in this computational

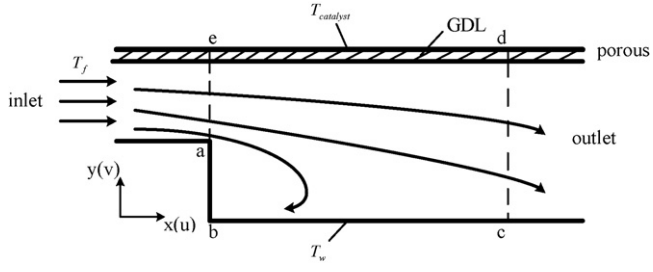

Fig. 2. Computational domain for fluid flow and heat transfer over backward facing step.

domain is given by:

$$\rho c_p \left(u\frac{\partial T}{\partial x} + v\frac{\partial T}{\partial y} \right) = \frac{\partial}{\partial x}\left(k\frac{\partial T}{\partial x} \right) + \frac{\partial}{\partial y}\left(k\frac{\partial T}{\partial y} \right) \quad (1)$$

The convective term in this equation can be re-written in the form of the inner product of the velocity vector and the temperature gradient, i.e.

$$\rho c_p(\vec{U} \cdot \mathrm{grad}T) = k\nabla^2 T \quad (2)$$

Integrating Eq. (2) over the computational domain shown in Fig. 2, and incorporating the Gauss law of reduction of integral dimensionality for the diffusion term, it can be shown that:

$$\int_{\Omega} \rho c_p(\vec{U} \cdot \mathrm{grad}T)\,\mathrm{d}A - \int_{cd} k\vec{n} \cdot \nabla T\,\mathrm{d}s - \int_{ea} k\vec{n} \cdot \nabla T\,\mathrm{d}s = \int_{abc} k\vec{n} \cdot \nabla T\,\mathrm{d}s + \int_{de} k\vec{n} \cdot \nabla T\,\mathrm{d}s \quad (3)$$

where ab, bc and de are the boundaries of the computational domain, and $\vec{n}$ is the outward normal to the computational domain boundary. The two terms on the right hand side of Eq. (3) represent the convective heat transfer rate at the interface between the fluid and the solid wall. Meanwhile, the first term on the left hand side of Eq. (3) indicates the energy transfer due to the motion of the fluid itself, while the second and third terms describe the heat conduction effect in the fluid. The inner product of the velocity vector and the temperature gradient is given by $(\vec{U} \cdot \mathrm{grad}T) = |\vec{U}||\vec{U}||\mathrm{grad}T| \cos\theta$, where θ is the local intersection angle between the local velocity vector and the temperature gradient. Hence, the value of the integration, i.e. the strength of the convective heat transfer, depends not only on the moduli of the velocity vector and the temperature gradient, respectively, but also on the included angle between them. Clearly, when the velocity vector and the temperature gradient are in full synergy, i.e. the included angle between them is 0°, the rate of heat transfer varies linearly with the temperature. Conversely, the convective heat transfer performance is reduced when the velocity vector and the temperature gradient intersect with an angle of more than zero degrees. Therefore, for a given flow rate and temperature difference between the fluid and the heat transfer surface, the degree of synergy between the velocity vector and the temperature gradient must be maximized in order to optimize the heat transfer effect.

To maximize the synergy of the two vector fields (i.e. the velocity vector and the temperature gradient) or the three scalar fields (i.e. the modulus of the velocity, the modulus of the temperature gradient, and the cosine of the included angle between them), it is necessary that (a) the intersection angle between the velocity vector and the temperature gradient is minimized, and (b) the three scalar fields all have high local values. A higher synergy among these three scalar fields results in a higher Nusselt number, i.e. an enhanced rate of heat transfer.

Tao et al. [15] showed that the three conventional methods for enhancing convective heat transfer, namely reducing the thickness of the thermal boundary layer, increasing the disturbance in the fluid, and increasing the velocity gradient at the solid wall, can be unified by the field synergy principle. In other words, all of these enhancement techniques involve reducing the intersection angle between the velocity vector and the temperature gradient [16].

3. Governing equations and boundary conditions

The governing equations for continuity, momentum, and energy in the computational domain shown in Fig. 2 are as follows:

Continuity equation:

$$\nabla \cdot V = 0 \quad (4)$$

Momentum equation:

(A) In the flow channel:

$$\rho u\frac{\partial u}{\partial x} + \rho v\frac{\partial u}{\partial y} = -\frac{\partial p}{\partial x} + \mu\left(\frac{\partial^2 u}{\partial x^2} + \frac{\partial^2 u}{\partial y^2} \right) \quad (5)$$

$$\rho u\frac{\partial v}{\partial x} + \rho v\frac{\partial v}{\partial y} = -\frac{\partial p}{\partial y} + \mu\left(\frac{\partial^2 v}{\partial x^2} + \frac{\partial^2 v}{\partial y^2} \right) \quad (6)$$

(B) In the gas diffusion layer:

$$\rho u\frac{\partial u}{\partial x} + \rho v\frac{\partial u}{\partial y} = -\frac{\partial p}{\partial x} + \mu\left(\frac{\partial^2 u}{\partial x^2} + \frac{\partial^2 u}{\partial y^2} \right) - \frac{\mu}{k}\varepsilon u \quad (7)$$

$$\rho u\frac{\partial v}{\partial x} + \rho v\frac{\partial v}{\partial y} = -\frac{\partial p}{\partial y} + \mu\left(\frac{\partial^2 v}{\partial x^2} + \frac{\partial^2 v}{\partial y^2} \right) - \frac{\mu}{k}\varepsilon v \quad (8)$$

Energy equation:

$$\rho u\frac{\partial T}{\partial x} + \rho v\frac{\partial T}{\partial y} = \Gamma\left(\frac{\partial^2 T}{\partial x^2} + \frac{\partial^2 T}{\partial y^2} \right) \quad (9)$$

where

$$\Gamma = \frac{k}{c_p} \quad (10)$$

The following parameters can be defined:

$$Re = \frac{\rho u_{\mathrm{m}} D_{\mathrm{h}}}{\mu} \quad (11)$$

$$Nu = \frac{h D_{\mathrm{h}}}{\lambda} \quad (12)$$

$$h = \frac{Q}{A\Delta T} \quad (13)$$

$$Q = \dot{m} c_p (T_{\mathrm{in}} - T_{\mathrm{out}}) \quad (14)$$

$$\Delta p = p_{\mathrm{in}} - p_{\mathrm{out}} \quad (15)$$

$$f = \frac{\Delta p}{1/2\rho u_{\mathrm{m}}^2} \cdot \frac{D_{\mathrm{h}}}{L} \quad (16)$$

$$\Delta T = \frac{T_{\max} - T_{\min}}{\log(T_{\max}/T_{\min})} \quad (17)$$

$$\theta = \cos^{-1}\left(\frac{U \cdot \nabla T}{|U||\nabla T|} \right) = \cos^{-1}\left(\frac{u(\partial T/\partial x) + v(\partial T/\partial y)}{|U||\nabla T|} \right) \quad (18)$$

$$\theta_m = \frac{\iint \theta \, dx \, dy}{\iint dx \, dy} \tag{19}$$

where u_m is the mean velocity in the minimum transverse area; D_h the inlet diameter; T_{in} and T_{out} the bulk temperatures of the channel inlet and channel outlet, respectively, T_w the temperature of the bipolar plate surface, and T_{max} and T_{min} are given by $T_{max} = \max(T_{in} - T_w, T_{out} - T_w)$ and $T_{min} = \min(T_{in} - T_w, T_{out} - T_w)$, respectively.

In the current problem, the fluid is cooled and the integral $\iint \rho c_p (U \cdot \nabla T) \, dx \, dy$ is less than zero. For convenience, a minus sign is added to the definition of the intersection angle in Eq. (18). Furthermore, when calculating the average synergy angle in Eq. (19), if the local synergy angle is larger than 90°, it is replaced by the angle $180^\circ - \theta$.

The current governing equations are elliptic partial differential equations, and hence boundary conditions are required for all of the boundaries of the computational domain. Due to the conjugated nature of the current problem, the bipolar plate surfaces are included within the solution domain and are treated as a particular type of fluid. The boundary conditions for the three regions of the computational domain are as follows:

1. At the inlet:

$$u = \text{const}, \quad T_{in} = \text{const}, \quad v = 0 \tag{20}$$

2. At the outlet boundary:

$$\frac{\partial u}{\partial x} = \frac{\partial v}{\partial x} = \frac{\partial T}{\partial x} = 0 \tag{21}$$

3. At the upper surface (porous surface):

$$u = v = 0 \tag{22}$$

$$T_{in} = T_{catalyst} = 353 \text{ K} \tag{23}$$

4. At the lower surface:

$$u = v = 0 \tag{24}$$

$$T = T_w \tag{25}$$

$$T_{in} > T_w \tag{26}$$

4. Solution strategy

Fig. 3 presents a flow chart of the current numerical modeling procedure. The PEMFC simulations were performed using the commercial CFD-RC software package. This package discretizes the mass, momentum and energy equations using the finite-volume semi-implicit method for pressure-linked equations consistent (SIMPLEC) method [17]. A detailed explanation of the various models of CFD-ACE is provided in [18]. In the simulations, it is assumed that the inlet section of the channel is hydro-dynamically fully developed. Hence, a fully developed velocity profile for rectangular ducts is imposed. A forced convection regime is imposed within the computational domain and the Navier–Stokes equations are solved under laminar assumptions. Prior to the simulations, a parametric study was performed to identify a suitable grid mesh capable of accurately modeling the thermal and velocity gradients near the walls. A spatial resolution of 302 × 32 meshes was found to be sufficient. In the simulations, the iterative computations were terminated once the residues were less than 10^{-8}. The CPU used a PC with a 3.2 GHz Intel Pentium 4 CPU, 1 GB DDR RAM, and the Windows XP operating system.

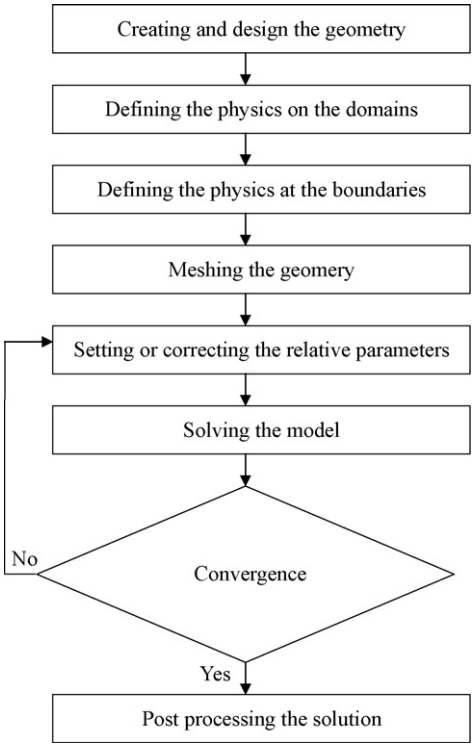

Fig. 3. Flow chart of numerical simulations.

5. Results and discussion

5.1. Velocity field

The flow simulations were performed using the non-uniform rectangular mesh (302 × 32) shown in Fig. 4. The Reynolds number (Re) of the flow was defined as $U_{in} D_h / v$, where U_{in} is the maximum velocity in the inlet. Fig. 5 shows the vertical velocity profile of the flow in a straight gas flow channel for laminar flow with $Re = 200$. Meanwhile, Fig. 6 illustrates the vertical velocity profile of the flow in the proposed gas flow channel with a wave-like form. Comparing Fig. 6 with Fig. 5, it is apparent that the periodic wave-like structure of the proposed gas flow channel increases the velocity in the vertical direction in the channel. Hence, the catalysis reaction in the catalyst layer is enhanced, thereby improving the performance of the PEMFC.

The pressure drop in the gas flow channel of the PEMFC is related to the Darcy friction factor, which is defined as:

$$f = -\frac{2 D_h}{\rho U_m^2} \left(\frac{dp}{ds} \right) \tag{27}$$

where ρ is the hydrogen density, U_m the mean channel velocity, and dp/ds is the local pressure gradient along the curvilinear

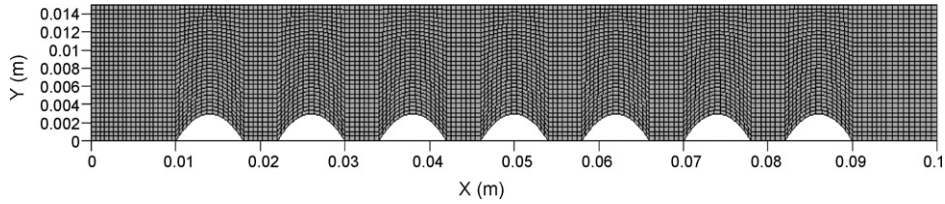

Fig. 4. Uniform mesh for bipolar plate flow field simulations.

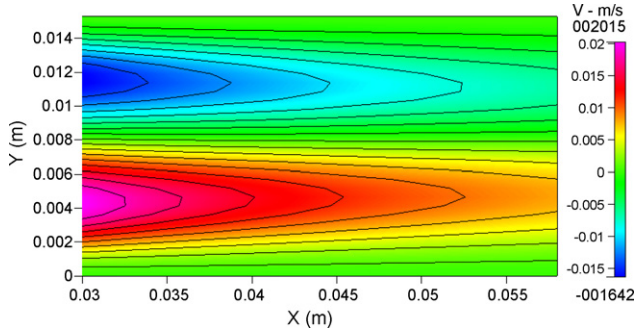

Fig. 5. Velocity field in conventional gas flow channel with straight geometry.

coordinate of the gas flow channel. Since this parameter is Reynolds number dependent, it is preferable to calculate the product *fRe*. Fig. 7 compares the variation of *fRe* with the curvilinear coordinate for the straight gas flow channel and for the novel gas flow channel with a wave-like form. Note that the Reynolds number of the flow is 200 in both cases. Since a fully developed velocity profile is imposed at the inlet boundary of the computational domain, the quantity *fRe* in the straight channel has an asymptotic form and approaches a value of 64. This value is consistent with the theoretical value of $fRe = 64$ for fully developed pipe flow. The good agreement between the two results validates the current numerical procedure. It can be seen that the wave-like geometry of the proposed gas flow channel increases the pressure drop within the channel compared to the straight channel. When the gas is first introduced into the channel, a high-pressure drop is generated when the flow encounters the first wave-like form. However, as the gas moves along the channel, the pressure drop reduces and the value of *fRe* varies periodically in accordance with the periodic surface of the gas flow channel. After the initial flow establishment region, the

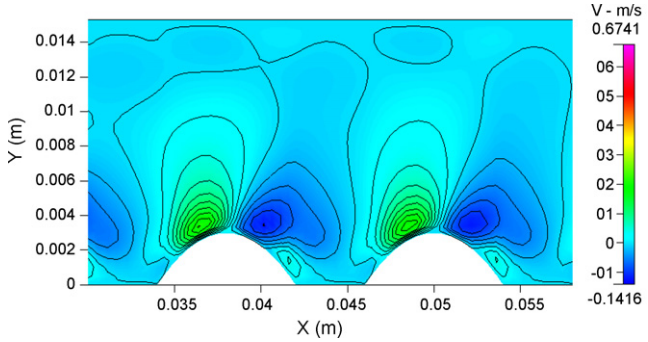

Fig. 6. Velocity field in gas flow channel with novel periodic wave-like form geometry.

average value of *fRe* in the gas flow channel with a wave-like geometry is found to be 102, i.e. 1.6 times higher than that in the conventional channel with a straight geometry.

Fig. 8 illustrates the velocity field in the wave-like form channel in the vertical directions. The results reveal that for an inlet velocity of 1.4 ms, the maximum *x*-direction velocity is 2.234 ms, while the maximum *y*-direction velocity is 0.6741 ms. It is apparent that the wave-like form channel induces a higher velocity in the *y*-direction than the straight channel, and hence the catalysis reaction performance in the catalyst layer is improved.

5.2. Temperature field

The thermal performance of the two gas flow channel geometries was initially characterized in terms of the evolution of the convective heat transfer coefficient, *Nu*, along the curvilinear coordinate:

$$Nu = \frac{h \cdot D_h}{k} = \frac{-D_h \cdot \partial T/\partial y|_{y=0}}{(T_{in} - T_w)} \tag{28}$$

where $T_{in} = 353$ K is the bulk mean fluid temperature over the cross-sectional area of the gas flow channel, T_w the channel wall temperature, and D_h is the hydraulic diameter. Figs. 9 and 10 shows the temperature distributions in the straight gas flow channel and the gas flow channel with a wave-like geometry, respectively. In both cases, the flow is laminar with a Reynolds number of $Re = 200$. Comparing the two figures, it is evident that the channel with a wave-like form has a lower and more

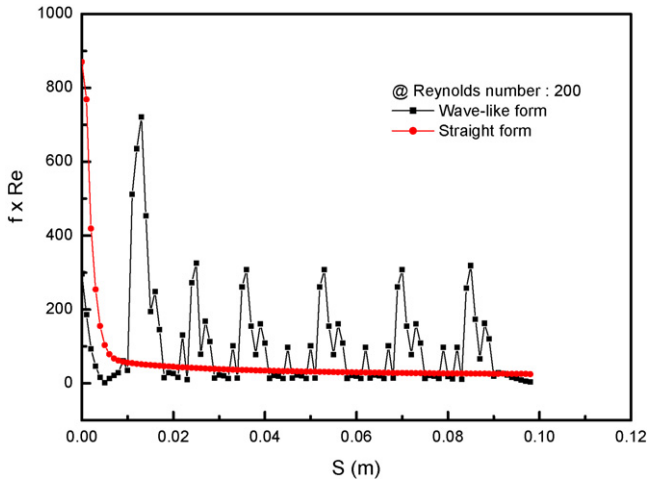

Fig. 7. Evolution of *fRe* term with curvilinear coordinate for two gas flow channel geometries (straight and wave-like).

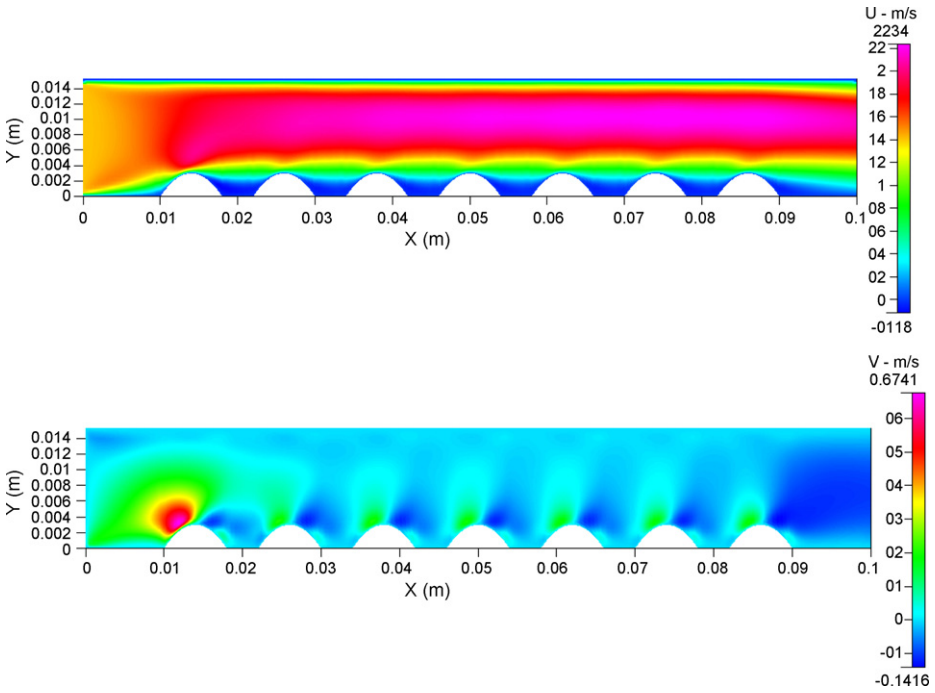

Fig. 8. Enhanced gas flow velocity fields in gas flow channel with wave-like form geometry.

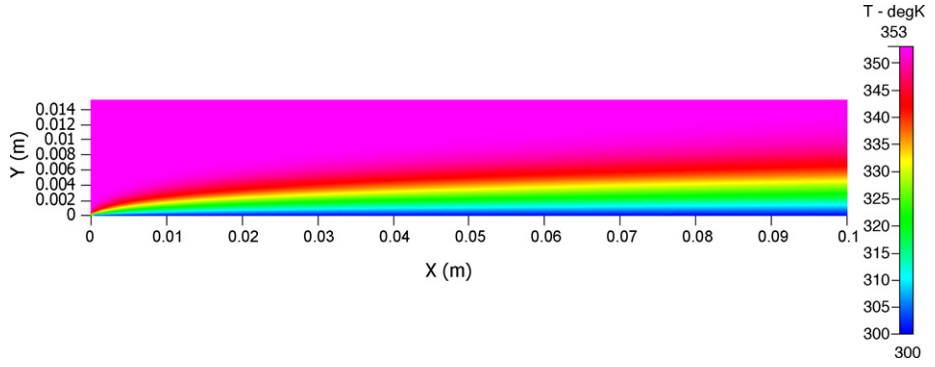

Fig. 9. Temperature field in conventional gas flow channel with straight geometry field.

uniform temperature, i.e. the bipolar plate with a periodic wave-form surface results in an improved heat transfer performance.

Fig. 11 presents the evolution of the Nusselt number with the curvilinear coordinate in the straight channel and in the novel wave-like form channel for a Reynolds number of 200. In the straight channel, the Nusselt number exhibits a classical power-law reduction and asymptotically approaches a value of $Nu = 3.2$, with an average Nusselt number of 4.2. This value is consistent with the results presented in the literature [19–20] and therefore validates the present CFD-ACE computations.

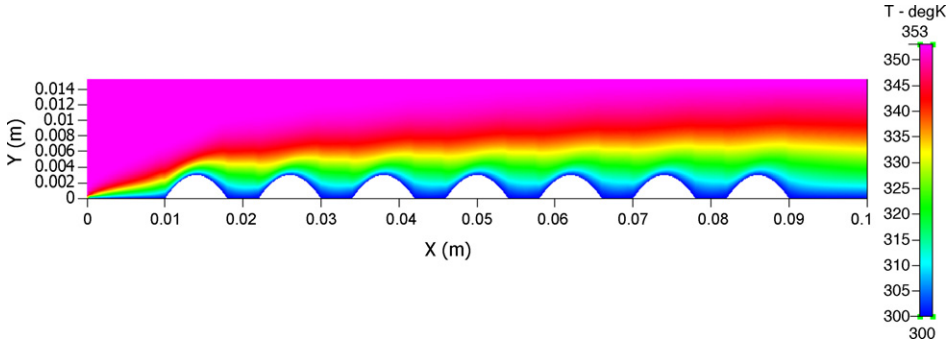

Fig. 10. Temperature field in gas flow channel with novel periodic wave-like form geometry.

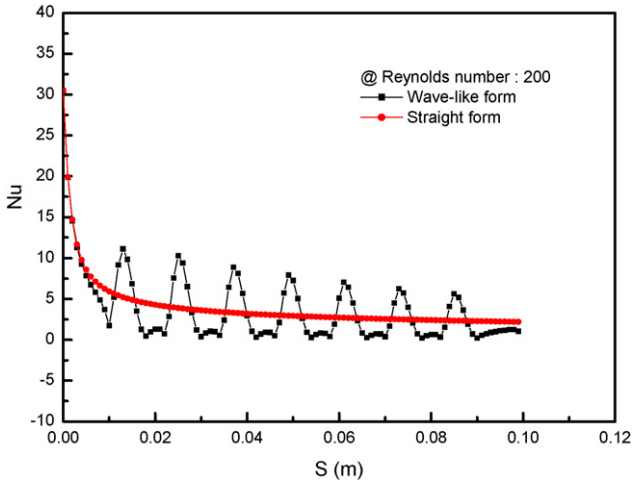

Fig. 11. Evolution of Nusselt number with curvilinear coordinate for two gas flow channel geometries (straight and wave-like).

In the gas flow channel with a wave-like form, a significant reduction in the Nusselt number is observed in the entrance region of the channel. However, the Nusselt number subsequently exhibits a periodic variation with a mean value of 7.5. It is apparent that the wave-like geometry enhances the heat transfer performance by a factor of approximately two compared to the conventional straight channel. The heat transfer enhancement is due to the presence of Dean vortices induced in the flow as it passes over the undulating surface of the gas flow channel.

5.3. Evaluation of enhanced convective heat transfer in wave-like form gas channel from field synergy effect perspective

Fig. 12 shows the variation of the Nusselt number with the Reynolds number in the straight and wave-like form gas flow channels, respectively. It is observed that the wave-like geometry enhances the thermal performance of the gas flow channel, particularly at higher Reynolds numbers. At a value of Re =200 (i.e. the Reynolds number considered in the present simulations), the wave-like geometry increases the value of Nu by approximately 20%. In general, an improvement in the single-phase convective heat transfer in a gas flow channel may be the result of an increased flow interruption, a reduction in the thermal boundary layer, or an increased velocity gradient near the solid channel wall.

The improvement in the heat transfer performance provided by the proposed wave-like form gas flow channel can be evaluated from the field synergy principle perspective, which states that the heat transfer is optimized when a good synergy is obtained between the velocity vector and the temperature gradient. Under the field synergy principle approach, the heat transfer performance of the gas flow channel is evaluated not in terms of the Nusselt number, but in terms of the intersection value (see Eq. (18)) and average intersection angle of the velocity vector and the temperature gradient.

Eq. (29) provides a meaningful insight into potential strategies for improving the convective heat transfer. It is evident that the heat transfer can be enhanced in one of three different ways, namely increasing the Reynolds and Prandtl numbers of the flow, increasing the fullness of the velocity and temperature profiles, or reducing the included angle between the velocity vector and the temperature gradient.

$$Re\,Pr \int (\vec{V} \cdot \nabla T)\,\mathrm{d}y = Nu \tag{29}$$

$$\vec{V} \cdot \nabla T = |\vec{V}||\nabla T| \cos\theta \tag{30}$$

Let θ_m be the average included angle between the velocity vector and the temperature gradient in the computational domain. Furthermore, if the local value of θ is greater than 90°, let its value be taken as $(180^\circ - \theta)$ when added to the summation of the included angle. Fig. 13 shows the variation of the average included angle with the Reynolds number for the straight gas flow channel and for the channel with the wave-

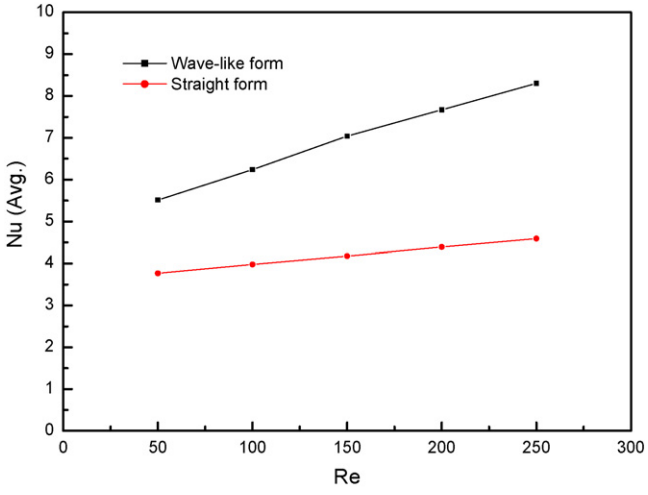

Fig. 12. Variation of average Nusselt number with Reynolds number in two gas flow channel geometries (straight and wave-like).

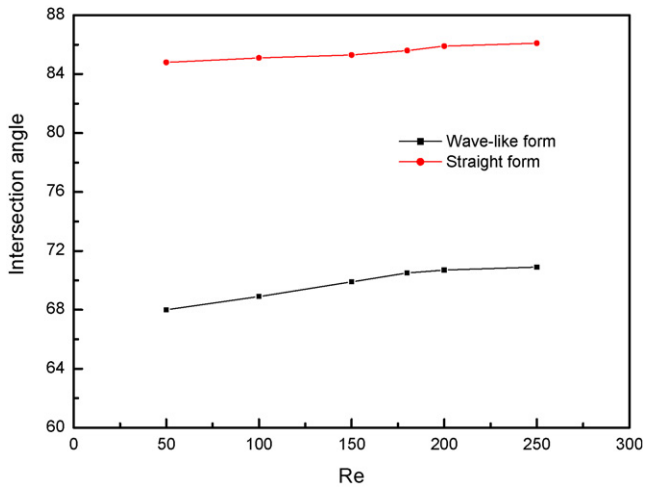

Fig. 13. Variation of average intersection angle with Reynolds number in two gas flow channel geometries (straight and wave-like).

like form geometry. At the value of $Re = 200$ considered in the present simulations, the intersection angle of the velocity vector and the temperature gradient in the straight channel is 87°. However, in the gas flow channel with the wave-like form geometry, the intersection angle is reduced to 70.5°. In other words, the flow interruption introduced by the wave-like form geometry causes the velocity vector and the temperature gradient to be more closely aligned. Hence, the enhanced convective heat transfer performance of the gas channel with the wave-like form geometry observed in Fig. 12 is consistent with the predictions of the field synergy principle.

6. Conclusions

This study has simulated low Reynolds number laminar flow in the gas flow channel of a PEMFC. The heat transfer performance and enhanced gas flow velocity characteristics of two different channel geometries have been considered, namely a conventional straight gas flow channel and a gas flow channel with a novel periodic wave-like geometry. The results have shown that compared to the conventional gas flow channel, the novel gas flow channel proposed in this study provides a significantly improved convective heat transfer performance and a higher gas flow velocity, and hence an improved catalysis reaction performance in the catalyst layer. The numerical results for the velocity and temperature fields within the two channels are in good agreement with the results presented in the literature. Finally, the enhanced performance of the proposed gas flow channel has been evaluated by calculating the average included angle between the velocity vector and the temperature gradient in the two gas flow channels. As predicted by the field synergy principle, the results have shown that the included angle in the flow channel with the wave-like form geometry is lower than that in the conventional straight channel. Hence, the field synergy principle provides an alternative to the Nusselt number when evaluating the thermal efficiency of gas flow channels in PEMFCs.

Acknowledgment

This research was supported by the National Science Council of Taiwan under contract No. NSC 94-2212-E-006-019.

References

[1] S. Srinivasan, D.J. Mankoo, H. Koch, M.A. Enayetullah, J. Power Sources 29 (1988) 367.
[2] T.E. Springer, T.A. Zawodinski, S. Gottesfeld, J. Electrochem. Soc. 136 (1991) 2334.
[3] D.M. Bernardi, M.W. Verbrugge, J. Electrochem. Soc. 139 (1992) 2477.
[4] K. Broka, P. Ekdunge, J. Appl. Electrochem. 27 (1997) 281.
[5] Z.M. Wang, C.Y. Wang, K.S. Chen, J. Power Sources 37 (2000) 1151.
[6] T. Berning, D.M. Liu, N. Djilali, J. Power Sources 106 (2002) 284.
[7] W.K. Lee, S. Shi'palee, J.W. Van Zee, J. Electrochem. Soc. 150 (2003) A341.
[8] S. Um, C.Y. Wang, J. Power Sources 125 (2004) 40.
[9] H. Meng, C.Y. Wang, J. Electrochem. Soc. 151 (2004) A358.
[10] Z.Y. Guo, D.Y. Li, B.X. Wang, Int. J. Heat Mass Transfer 41 (1998) 2221.
[11] S. Wang, Z.X. Li, Z.Y. Guo, Proceeding of 11th IHTC, vol. 5, 1998, p. 405.
[12] W.Q. Tao, Y.L. He, Q.W. Wang, Z.G. Qu, F.Q. Song, Int. J. Heat Mass Transfer 45 (2002) 4871.
[13] W.Q. Tao, Z.Y. Guo, B.X. Wang, Int. J. Heat Mass Transfer 45 (2002) 3849.
[14] C.C. Wang, C.K. Chen, Int. J. Heat Mass Transfer 45 (2002) 2587.
[15] W.Q. Tao, Y.L. He, Q.W. Wang, Z.G. Qu, F.Q. Song, Int. J. Heat Mass Transfer 45 (2002) 4879.
[16] Y.L. He, W.Q. Tao, F.Q. Song, W. Zhang, Int. J. Heat Fluid Flow 26 (2005) 459.
[17] S.V. Patankar, Numerical Heat Transfer, Hemisphere, Washington, DC, 1980.
[18] CFD Research Corp., CFD-ACE (U)^{TM} User Manual, version 2002, 2002, Huntsville, Alabma.
[19] Z.Y. Guo, D.Y. Li, B.X. Wang, Int. J. Heat Mass Transfer 41 (1998) 2221.
[20] Y. Lasbet, B. Auvity, C. Castelain, H. Peerhossaini, J. Power Sources 156 (2006) 114.